Industry Science and Engineering Vol. 3 No. 9, 2026

Mechanical Behavior Analysis of Wire Rope in Swabbing and Drainage Systems

Dan Li[1,2], Jie Fan[1,2], Guangchun Liu[2,3], Ping Chen[1,2], Qiguo Fan[2,3], Wenxue Jiang[1,2], Shaohu Liu[4,5], Lei Zhang[4,5,*]

[1]*Drilling and Production Engineering Technology Research Institute, CNPC Chuanqing Drilling Engineering Co., Ltd., Xi'an, Shaanxi, China*

[2]*National Engineering Laboratory for Exploration and Development of Low-Permeability Oil and Gas Fields, Xi'an, Shaanxi, China*

[3]*Changqing Downhole Technology Operation Company, CNPC Chuanqing Drilling Engineering Co., Ltd., Xi'an, Shaanxi, China*

[4]*School of Mechanical Engineering, Yangtze University, Jingzhou, Hubei, China*

[5]*National Key Laboratory of Low-Carbon Catalysis and Carbon Dioxide Utilization, Wuhan, Hubei, China*

**Corresponding Author*

Abstract: To assess the operational safety of wire ropes under the complex operating conditions of a swabbing and drainage system, this study investigates the stress distribution, deformation, and contact behavior of a 6×19FS+IPS wire rope under axial tension and bending over a sheave. A three-dimensional finite element model incorporating the fiber core, strands, and their contact interactions is developed. Axial tension and bending-contact analyses are performed at loads of 10-80kN to obtain the von Mises stress, strain, total deformation, and normal contact pressure. At an axial load of 80kN, the maximum von Mises stress is 1171.8MPa and the maximum total deformation is 3.98mm. Localized high stresses occur in the inner wires and interstrand contact regions. When the axial load increases from 30kN to 40kN, the maximum von Mises stress and contact stress increase significantly. The maximum von Mises stress rises from 104.12MPa to 376.19MPa. The contact stress increases from 175.17 to 474.36MPa. Under the 80kN bending condition, the maximum von Mises stress, principal strain and normal contact pressure reach maximum values at the mid-bending section. The values are 1042MPa, 0.0131 and 878.15MPa, respectively. The wire rope meets the strength requirements at the maximum working load. However, non-uniform force and local stress concentration occur in the inner wires, interstrand contact regions and bending segment around the sheave. The contact response under high loads should be given attention in engineering application to reduce the risk of accidents.

Keywords: Swabbing and Drainage System; Wire Rope; Mechanical Behavior; Finite Element Analysis; Axial Tension

1. Introduction

Swabbing and liquid drainage is a common operation used to restore wellbore flow capacity during workover and well testing. As shown in Figure 1, a workover rig drum drives the wire rope, which passes over a fixed sheave and through the wellhead guide to connect to a downhole swab. Reciprocating motion lifts accumulated liquid from the wellbore. In addition to transmitting power, the wire rope undergoes drum winding, redirection over sheaves, and shocks during starting and stopping. Overall tension, bending fatigue, interwire fretting wear, and corrosion can cause wire rope failure.

A wire rope is a spatial helical structure formed by laying multiple layers of steel wires according to a specified pattern. Its load-carrying capacity depends on the wire material properties, interstrand contact conditions, friction coefficients, and boundary constraints. Compared with a homogeneous rod, a wire rope exhibits pronounced geometric nonlinearity, contact nonlinearity, and structural anisotropy under axial tension and bending. In terms of analytical theory, Chen [1] developed a mechanical analysis model for helical wire ropes.

The steel wires were treated as spatial helical rods or helical beams. The deformation and internal force responses of the strand under axial load and torque were derived through geometric compatibility relations and mechanical equilibrium equations. Utting and Jones [2,3] combined theoretical analysis with axial tensile tests. They studied the force-displacement response of independent strands under axial load, the deformation compatibility of steel wires, and the load distribution law. The studies showed that the actual stress state of helical steel wires was not simple uniaxial tension. It consisted of axial tension, bending and torsion. Contact and relative slip between wires further changed the overall stiffness of the strand and the local stress distribution. Cardou and Jolicoeur [4] provided a systematic overview of early theories on helical strands. They pointed out the limitations of analytical models under complex cross-sections, irregular contact, and large deformation conditions.

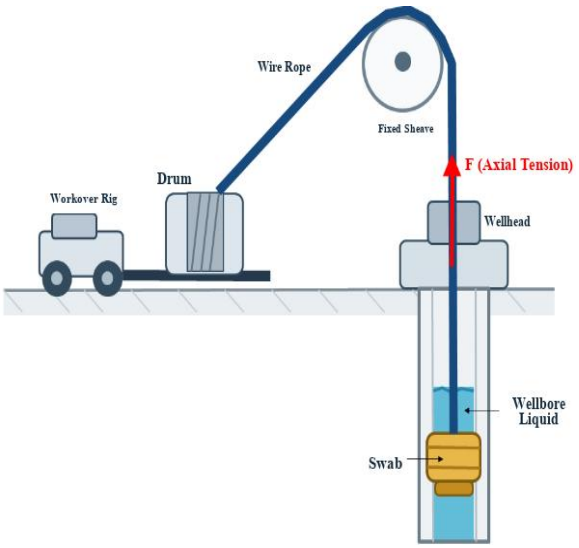


Figure 1. Schematic of Swabbing and Drainage System

With the improvement of numerical computing capability, research focus has shifted to local stress and contact behavior. Jiang [5], Nawrocki and Labrosse [6] proposed finite element modeling methods for straight strands. They built the real helical geometry of wires and defined inter-wire contact. On this basis, they analyzed the stress distribution, contact pressure and relative slip characteristics of wires in each layer under axial load.

In addition to axial tension, bending-contact coupling also affects wire rope reliability when ropes pass over sheaves. Ridge [7] studied the effects of degradation quality and damage state on the fatigue performance of wire ropes. The results show that wire ropes undergo progressive accumulation of wire wear, local plastic deformation and wire breakage damage during repeated bending. Usabiaga [8] measured the normal and tangential line contact pressure at the wire rope–sheave interface through experiments. They revealed the non-uniform distribution of contact pressure along the wrap angle direction. Ma [9] developed a computer-aided model for wire ropes passing over sheaves. The model describes the geometric configuration and contact relationships of the rope along a curved path. Shi [10] studied the rope–sheave traction interface. They analyzed the effects of wrap angle, friction and traction force transmission on the interface contact state. These studies show that axial tension sets the overall pre-tension. Sheave curvature adds bending stress. Radial compression redistributes contact pressure between wires and at the rope–sheave interface. Thus, the sheave-wrapping case cannot be simplified as straight-rope axial tension.

Researchers in China have further extended studies on internal forces in helical strands, 3D contact finite element modeling, bending response of shaped strands and fatigue damage evaluation [11-19]. Although wire ropes are well studied via theory, simulation and experiments, their loading in swabbing and drainage systems differs from these conventional cases. In addition to the constant weight of the swab, the suspended rope weight and the weight of the wellbore liquid column vary dynamically during operation. Existing studies tend to simplify the wire rope as a straight model, with insufficient consideration of coupled friction and compression between strands and between wires. To address these issues, this study considers a 6×19FS+IPS wire rope used in a swabbing and drainage system. Geometric models are established for strand centerlines and the double-helical trajectories of wires within each strand. Rope deformation, von Mises stress, and contact pressure are investigated at different loads under axial tension and coupled bending-contact over a sheave. The locations of stress concentrations and their evolution with increasing load are identified.

2. Wire Rope Geometry and Structural Equations

The 6×19FS+IPS wire rope consists of a fiber core and six steel strands, each containing 19

wires arranged in a double-helical structure, as shown in Figure 2. This construction is suitable for heavy-duty applications requiring wear resistance.

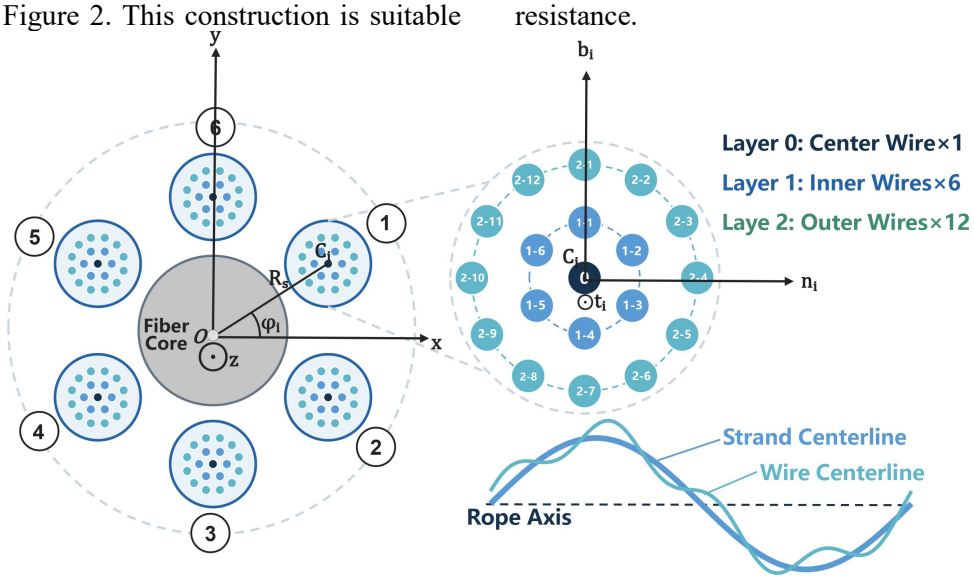


Figure 2. Structure of 6×19FS+IPS Wire Rope

A Cartesian coordinate system Oxyz is defined in Figure 2, with the z-axis coinciding with the center axis of the straight rope and directed out of the page. The centerline coordinates of strand i (i = 1, 6) are expressed as:

$$\begin{cases} C_i(\theta) = \left[R_s\cos(\theta+\varphi_i) \quad R_s\sin(\theta+\varphi_i) \quad h_r\theta\right]^T \\ \varphi_i = 2\pi(i-1)/6 \\ h_r = \dfrac{P_r}{2\pi} \end{cases} \tag{1}$$

Where R_s is the radial distance from the outer strand center to the rope axis (m); P_r is the rope lay length, defined as the axial distance advanced along z during one complete revolution of an outer strand around the core (m); and θ is the rope helical phase parameter (rad).

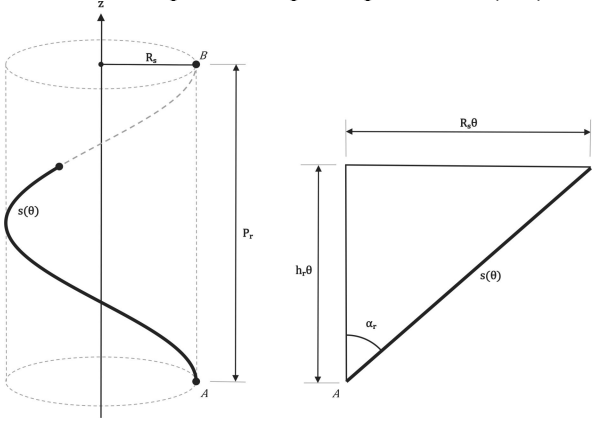


Figure 3. Helical Centerline and Unwrapped Geometry of an Outer Strand

As shown in Figure 3, the arc length s of an outer strand centerline and the rope lay angle α_r are given by:

$$\begin{cases} s(\theta) = \sqrt{(R_s^2 + h_r^2)\theta} \\ \alpha_r = \arctan\left(\dfrac{2\pi R_s}{P_r}\right) \end{cases} \tag{2}$$

The tangent vector t_i, normal vector n_i, and binormal vector b_i are constructed along the outer strand centerline (Figure 2). The centerline of wire k in layer j is represented by a nested helix. Its spatial position and phase angle are expressed as:

$$\begin{cases} r_{ijk}(\theta) = C_i(\theta) + \rho_j[\cos\psi_{jk}(s)n_i(\theta) + \sin\psi_{jk}(s)b_i(\theta)] \\ \psi_{jk}(s) = \eta_j\left(\dfrac{2\pi s}{P_{s,j}}\right) + \dfrac{2\pi k}{N_j} + \psi_{j,0} \end{cases} \tag{3}$$

Where ρ_j, $P_{s,j}$, and N_j denote the helical radius (m), strand lay length (m), and number of wires in layer j, respectively. The parameter $\eta_j = \pm 1$ specifies the lay direction: a positive sign indicates that the phase increases with s, whereas a negative sign indicates that it decreases with s. The initial phase $\psi_{j,0}$ adjusts the arrangement of wires in layer j in the initial cross section.

The nominal rope diameter is D=16 mm. The rope lay length is calculated as:

$$T = K \times D \tag{4}$$

Where K is the lay-length factor, assigned the conventional value of 7. The resulting rope lay length is 112mm.

3. Finite Element Model Parameters

3.1 Material Properties and Basic Assumptions

Steel strand wires are modeled as linearly elastic high-carbon steel, and the fiber core as an

equivalent continuum [20,21]. Table 1 lists the material properties. To ensure consistency between the mathematical and finite element models, the following assumptions are made: (1) steel wires are isotropic and linearly elastic[22-24]; (2) unilateral frictional contact permitting separation acts between wires and between the wire rope and the sheave groove [25]; and (3) manufacturing residual stresses, plasticity, wear, and corrosion are neglected.

Table 1. Material Properties of Wire Rope

Component	Material	Young's Modulus E (GPa)	Poisson's Ratio μ	Density ρ (kg·m^{-3})	Constitutive Model
Steel Strands	High-Carbon Steel	210	0.30	7850	Linear Elasticity
Fiber Core	Equivalent Continuum	6	0.40	1400	Equivalent Isotropic Material

3.2 Boundary Conditions

For axial tension, frictional contact is defined between wires. The wire-wire friction coefficient is 0.10, and the coefficient between steel wires and the impregnated fiber core is 0.05. One end of the rope is constrained, while a tensile load of 10-80kN is applied along the rope center axis at the other end.

The bending-tension model of the rope over a sheave uses a general contact algorithm to automatically identify potentially changing contact relationships between neighboring strands and between the rope and the sheave groove. The normal contact behavior is represented by hard contact, which permits separation as the load decreases and prevents interpenetration under compression, thereby transmitting normal contact pressure. Tangential behavior follows a Coulomb friction model with a coefficient of 0.10.

3.3 Meshing and Mesh Independence

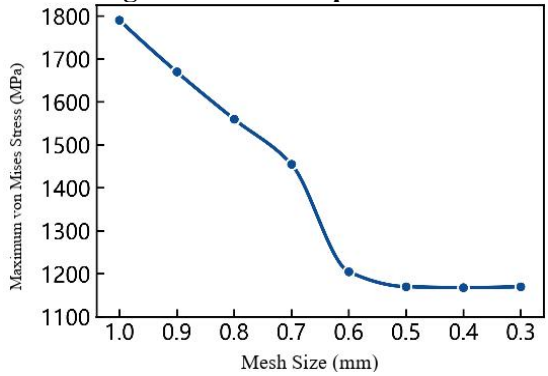
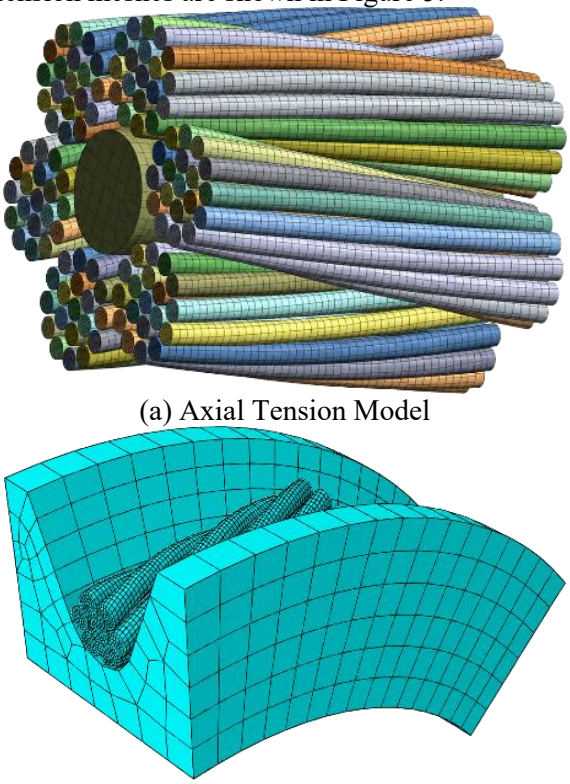


Figure 4. Results of Mesh Independence Study

The mesh size affects both computational accuracy and efficiency. Hexahedral elements are used. The mesh independence study in Figure 4 shows that the results stabilize at an element size of 0.5mm. Accordingly, a 0.5mm mesh is used for the wire rope in subsequent simulations, and a 5mm mesh is used for the sheave. The axial tension and sheave bending-tension meshes are shown in Figure 5.



(a) Axial Tension Model

(b) Bending-Tension Model over a Sheave

Figure 5. Finite Element Meshes of the Wire Rope

4. Analysis of Wire Rope Mechanical Behavior

4.1 Mechanical Response under Axial Tension

During upward and downward swabbing operations, both the suspended weight of the rope and the pressure of the downhole liquid column vary continuously. Using the mesh in Figure 5(a), one end is fixed and external loads of 10-80kN are applied at the other. The resulting mechanical responses include von Mises stress, strain, normal interwire contact stress, and sliding displacement.

Figure 6 shows the von Mises stress distribution

at the maximum load of 80kN, with a peak value of 1171.8MPa. High stresses are mainly concentrated in portions of the outer steel strands adjacent to the fiber core. Under axial tension, the helically laid wires press against surrounding wires and are constrained by neighboring wires, concentrating contact loads locally. The von Mises stress also decreases progressively along the overall rope axis. As shown in Figure 7, the steel wires carry most of the stress in the local inner-wire/fiber-core model. Because the elastic modulus of the fiber core is much lower than that of the steel wires, the core deforms more readily under compression and cushions the contact stresses.

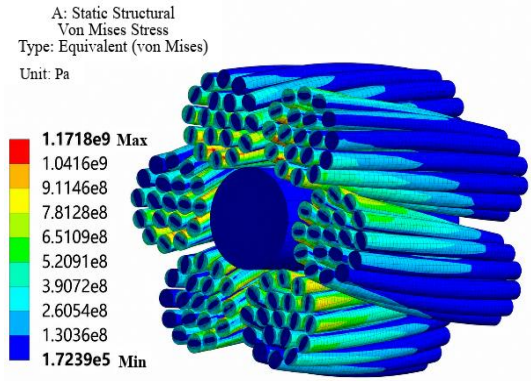


Figure 6. Von Mises Stress in the Wire Rope under Axial Tension

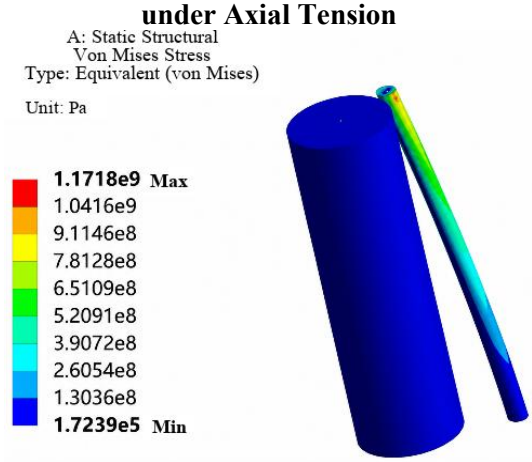
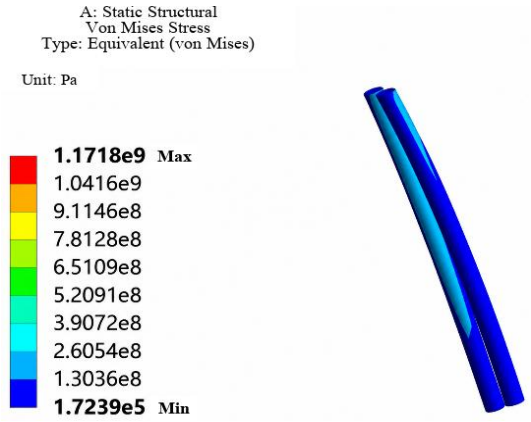
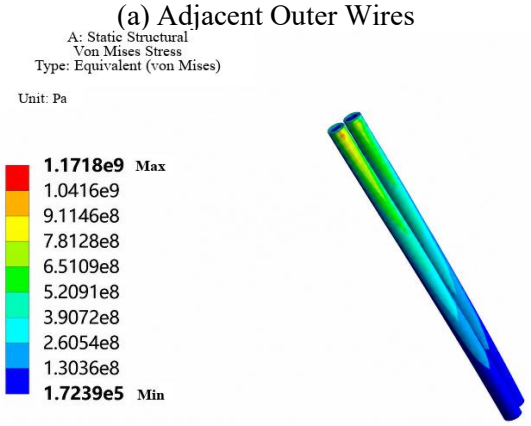


Figure 7. Von Mises Stress in the Inner Wires and Fiber Core

The stress contours for adjacent outer and inner wires are extracted in Figure 8. Outer wires show lower stress because they are less constrained by surrounding wires. Differences in wire position and contact state cause local load redistribution. Inner wires are compressed and constrained. Local contact also occurs as axial load transfers through the twisted structure, producing larger stress regions.



(a) Adjacent Outer Wires



(b) Adjacent Inner Wires

Figure 8. Von Mises Stress in Adjacent Steel Wires

Under 80kN axial load, total deformation shows a clear gradient along the rope length in Figure 9. Displacement is limited at the constrained end and accumulates toward the loaded end. Deformation at the loaded end varies markedly among wires. This relates directly to helical arrangement, inter-strand contact and load distribution. Deformation increases closer to the fiber core. The maximum is 3.98mm at the innermost wire end.

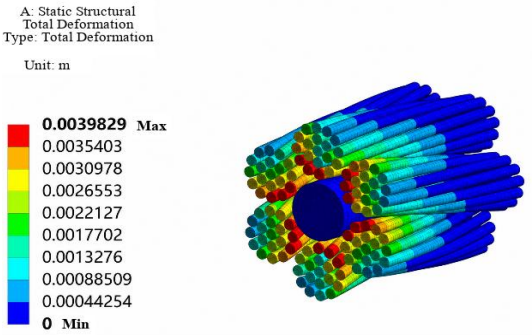


Figure 9. Total Deformation of Wire Rope

The von Mises stress, total deformation, strain, and contact stress of the wire rope under different loads are plotted in Figure 10. As the axial load increases from 10kN to 80kN, all four parameters increase continuously. The total

deformation increases from 0.17 to 3.98mm. The strain increases from 0.0039 to 0.0137. At 30–40kN, von Mises stress and contact stress rise from 104.12 to 376.19MPa and from 175.17 to 474.36MPa, respectively. Both grow non-uniformly with load.

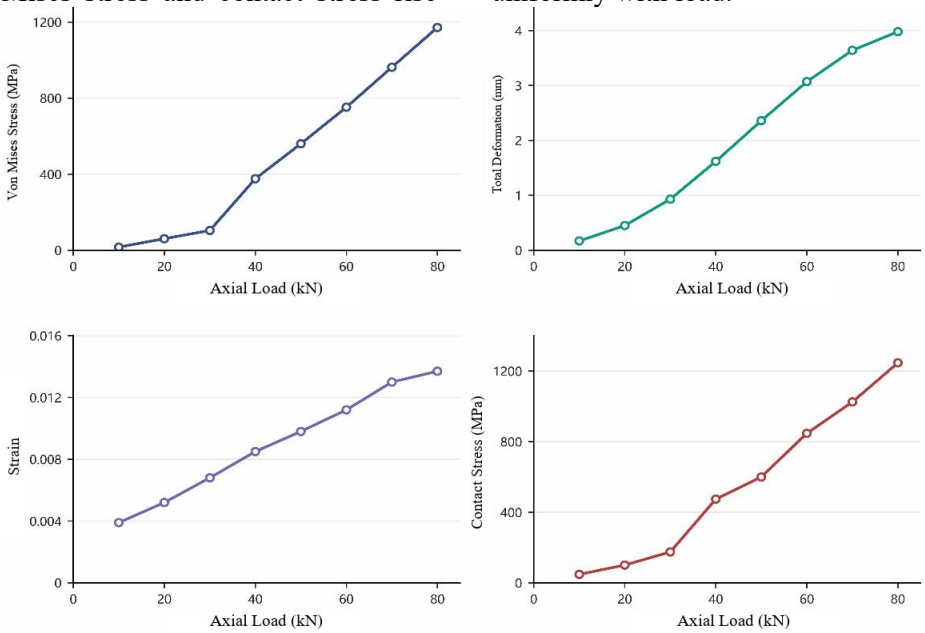


Figure 10. Axial Load versus Mechanical Response of Wire Rope

4.2 Mechanical Response under Bending

Bending load is a main load form for wire ropes working on sheaves and drums. It greatly increases the probability of mechanical damage. A rope-sheave model is considered. To improve efficiency, the model was simplified. Lay length and lay angle were retained. The 19-wire core was simplified to a single wire of equal diameter. Both rope ends were coupled to end-face nodes via reference points RP-1 and RP-2. Translation is constrained and rotation is released at RP-1, while an axial load of 10-80kN is applied at RP-2. The boundary conditions are shown in Figure 11.

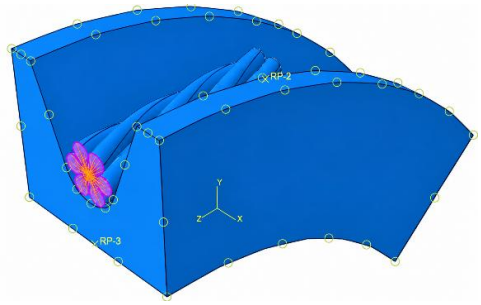


Figure 11. End Coupling and Boundary Conditions of Bending Model

At an axial load of 80kN, the wire rope bends along the sheave groove. The von Mises stress distribution is shown in Figure 12. The maximum stress is 1042MPa and occurs in the middle of the bend owing to the combined effects of axial tension, bending, wire-groove contact, and interwire compression. As the rope enters the bent segment, its radius of curvature and contact constraints change. Interstrand compression and friction redistribute loads among the wires, producing the highest local von Mises stress in the middle segment.

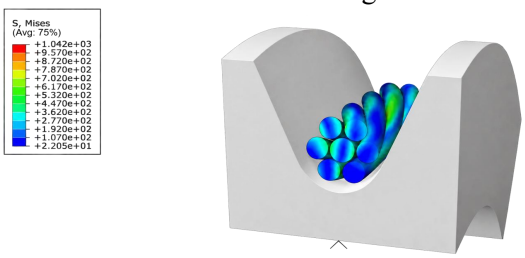


Figure 12. Von Mises Stress in Wire Rope under Bending

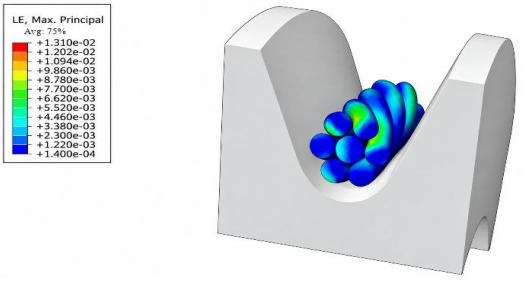


Figure 13. Strain in the Wire Rope under Bending

The maximum principal strain in Figure 13 is 1.31×10^{-2}. Combined axial tension and bending over the sheave groove cause different degrees of wire elongation at different locations. The helical structure, interwire contact, and contact with the groove alter local deformation,

increasing strain at the outer portions of the wires.

Figure 14 shows a maximum normal contact stress of 878.15 MPa, scattered at wire–wire compression zones. Differences in the contact positions and areas between wires and the groove, and between adjacent wires, result in a nonuniform distribution of normal loads.

As shown in Figure 15, the von Mises stress, strain, and contact pressure of the bent rope increase continuously as the load rises from 10 to 80kN, with larger increments at high loads. In particular, between 70 and 80kN, the von Mises stress increases from 406.7 to 1042MPa, and the contact pressure rises from 435.6 to 878.15MPa. These pronounced increases suggest possible changes in local contact conditions or strongly concentrated loading at high loads.

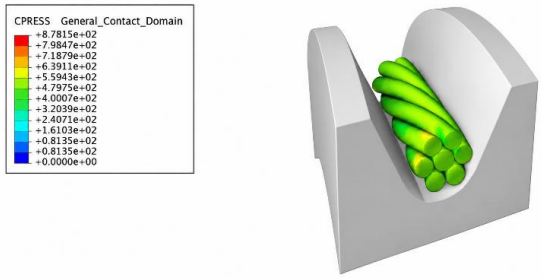


Figure 14. Normal Contact Pressure in Wire Rope under Bending

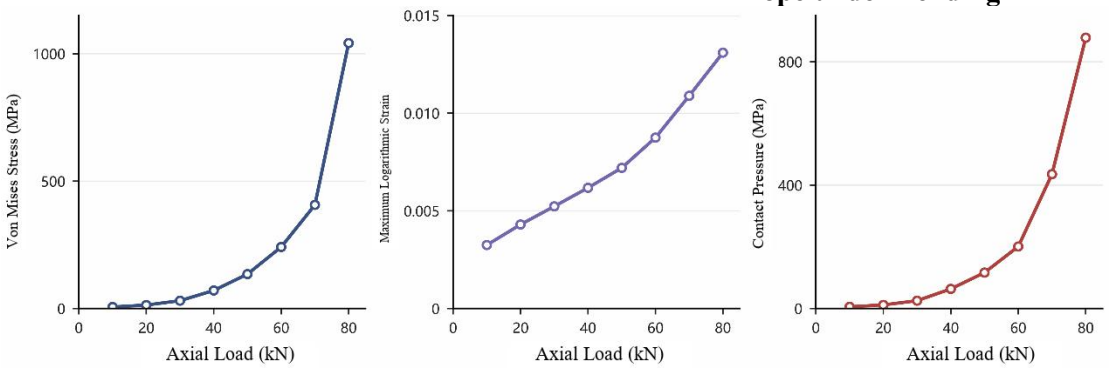


Figure 15. Applied Load versus Mechanical Response under Bending

5. Conclusions

The mechanical behavior of a 6×19FS+IPS wire rope operating under the complex conditions of a swabbing and drainage system was investigated. Analyses of stress, deformation, and contact responses under axial tension and bending over a sheave lead to the following conclusions:

(1) At the maximum axial operating load of 80kN, the maximum von Mises stress is 1171.8MPa, below the material allowable stress of 1775MPa adopted in the model. The maximum total deformation is 3.98mm. The rope therefore satisfies the overall static strength requirement.

(2) Under axial tension, loading within the rope is nonuniform. Inner wires and inter-strand contact zones show higher stress than outer regions because of load transfer, wire compression and contact constraints in the helical structure. As load increases, von Mises stress and contact stress grow non-uniformly. It indicates that local contact strongly affects the load-bearing response.

(3) Under bending over a sheave at the maximum operating load of 80kN, the maximum von Mises stress in the middle of the bend is 1042MPa, and the maximum normal contact pressure is 878.15MPa. The combined effects of axial tension, additional bending, groove contact, and interwire contact produce stress concentrations in the middle of the bend and at local contact sites. These regions should receive particular attention during operational inspection and condition monitoring.

Under the 80kN maximum working load with sheave bending, the mid-bending section shows a maximum von Mises stress of 1042MPa and a maximum normal contact pressure of 878.15MPa. Axial tension and additional bending act together. Contact occurs at the rope groove and between wires. These factors jointly cause stress concentration in the mid-bending section and local contact zones. These areas should be key targets for inspection and condition monitoring.

(4) Under bending, local mechanical response grows markedly at high load. From 70 to 80kN, the maximum von Mises stress rises from 406.7 to 1042MPa. The maximum contact pressure increases from 435.6 to 878.15MPa.

Future work can verify local stress and deformation via tensile and sheave-wrapping tests. Cyclic bending, start-stop impact, wear and corrosion should also be considered. These affect damage accumulation and service life. The

results support wire rope selection, condition monitoring, and design optimization in swabbing and drainage systems. This helps ensure safe and efficient workover operations.

Acknowledgments

This paper is supported the CNPC Commissioned Technology Development Project (No. CQZT-zcy-2025-JS-572).

References

[1] G. Chen. Mechanical Analysis of Wire Rope Winding State on Double Broken-line Drum. Coal Mine Modernization, 2025, 34(1):102-106,111.

[2] W. S. Utting, N. Jones. The Response of Wire Rope Strands to Axial Tensile Loads. Part I. Comparison of Experimental Results and Theoretical Predictions. International Journal of Mechanical Sciences, 1987, 29(9):605-619.

[3] W. S. Utting, N. Jones. The Response of Wire Rope Strands to Axial Tensile Loads. Part II. Comparison of Experimental Results and Theoretical Predictions. International Journal of Mechanical Sciences, 1987, 29(9):621-636.

[4] A. Cardou, C. Jolicoeur. Mechanical Models of Helical Strands. Applied Mechanics Reviews, 1997, 50(1):1-14.

[5] W. G. Jiang, M. S. Yao, J. M. Walton. A Concise Finite Element Model for Simple Straight Wire Rope Strand. International Journal of Mechanical Sciences, 1999, 41(2):143-161.

[6] A. Nawrocki, M. Labrosse. A Finite Element Model for Simple Straight Wire Rope Strands. Computers & Structures, 2000, 77(4):345-359.

[7] I. M. L. Ridge, C. R. Chaplin, J. Zheng. Effect of Degradation and Impaired Quality on Wire Rope Bending over Sheave Fatigue Endurance. Engineering Failure Analysis, 2001, 8(2):173-187.

[8] H. Usabiaga, M. Ezkurra, M. A. Madoz, et al. Experimental Test for Measuring Normal and Tangential Line Contact Pressure between Wire Rope and Sheaves. Experimental Techniques, 2008, 32(5):34-43.

[9] W. Ma, Y. X. Zhu, G. A. Chen. Computer-aided Modeling of Wire Ropes Bent over a Sheave. Advances in Engineering Software, 2015, 90:11-21.

[10] X. Shi, Y. Pan, X. Ma. Modeling and Analysis of the Rope-sheave Interaction at Traction Interface. Journal of Applied Mechanics, 2017, 84(3):031003.

[11] J. Ma, S. Ge, D. Zhang. Calculating Model and Numerical Simulation of Stress-strain Distribution of Wires Within Strands. Journal of Mechanical Engineering, 2009, 45(11):277-282.

[12] J. Ma, S. Ge, D. Zhang. Research on Three-dimensional Contact Model and Stress Distribution between Wires of Steel Strand. China Mechanical Engineering, 2012, 23(7):864-868.

[13] F. Meng, J. He, Y. Chen, et al. Analysis of Torsional and Bending Performances between Spiral Oval and Spiral Triangular Strand Ropes. Journal of Huazhong University of Science and Technology (Natural Science Edition), 2017, 45(3):8-16.

[14] Y. Chen, Z. Chen, P. Meng, et al. Comparative Study of Bending Performances of Spiral Triangular Strand and Simple Straight Strand Based on Finite Element Method. Journal of China University of Mining & Technology, 2015, 44(6):1105-1112.

[15] L. Li, H. Nie, X. Wei, et al. The Simulation Analysis of Mechanical Properties for the Arresting Cable. Machine Design and Manufacturing Engineering, 2023, 52(5):1-6.

[16] L. Zhang. Mechanical Characteristics and Failure Analysis of Elevator Triangular Traction Wire Rope. China Special Equipment Safety, 2024, 40(4):20-25.

[17] C. Xu, Y. Peng, Y. Wang, et al. Influence of Strand Structure on Fretting Friction and Wear Characteristics between Spiral Contact Steel Wires. Tribology, 2023, 43(10):1175-1188.

[18] H. Lu, Y. Li, M. Zhang, et al. Research Progress on Fretting Damage of the Flexible Multi-strand Wire Structure. Journal of Mechanical Strength, 2025, 47(12):48-57.

[19] S. Ma, H. Sun, Y. Zhang, et al. Review of Nondestructive Testing Technology for Wire Rope of Special Electromechanical Equipment. Mechatronics, 2021, 27(5):44-49.

[20] W. Zhang, W. Liu, C. Lv, et al. Research on Discontinuous Contact Intra-strand Steel Stress of Steel Rope Ring CVT. Journal of Mechanical Transmission, 2022, 46(8):100-104.

[21]B. Xu, L. Xiang, Z. Wang, et al. Elastoplastic Mechanical Behavior and Theoretical Model of Multi-layered Helical Wire Rope. Scientia Sinica (Physica, Mechanica & Astronomica), 2026, 56(6):139-162.

[22]M. Li, Y. Wu, Y. Chen, et al. Fine Finite Element Modeling Method of Steel Wire Braided Reinforced Hose Considering Contact Nonlinearity. Journal of Propulsion Technology, 2023, 44(1):206-214.

[23]J. Chen, B. Xu, L. Dai, et al. Mechanical Behavior and Deformation Mechanism of High-strength Metallic Wires. Chinese Science Bulletin, 2024, 69(21):3154-3176.

[24]J. Xi. Analysis of Influence of Drum Rope De-flection Angle and Rope Guide Block on Steel Rope Wear. Construction Machinery and Equipment, 2026, 57(3):74-78, 124-125.

[25]Z. Geng, X. Xue, S. Mäkimattila, et al. Tribological Behaviour of Pretension Steel Wire and Traction Wheel Material in Dry Sliding and Grease Lubrication Contacts. Lubrication Engineering, 2026, 51(3):48-54.